Multilayer Graphene as an Endoreversible Otto Engine

Nathan M. Myers *, Francisco J. Peña *, Natalia Cortés , Patricio Vargas

Posted Date: 7 April 2023

doi: 10.20944/preprints202304.0113.v1

Keywords: magnetic cycle; quantum Otto cycle; graphene; quantum thermodynamics

Article

Multilayer Graphene as an Endoreversible Otto Engine

Nathan M. Myers [1]*, Francisco J. Peña [2,3]*, Natalia Cortés[4,5] and Patricio Vargas [6]

[1] Department of Physics, Virginia Tech, Blacksburg, Virginia 24061, USA; myersn1@vt.edu
[2] Departamento de Física, Universidad Técnica Federico Santa María, Av. España 1680, Valparaíso 11520, Chile; francisco.penar@usm.cl
[3] Millennium Nucleus in NanoBioPhysics (NNBP), Av. España 1680, Valparaíso 11520, Chile
[4] Instituto de Alta Investigación, Universidad de Tarapacá, Casilla 7D, Arica, Chile
[5] Department of Physics and Astronomy, and Nanoscale and Quantum Phenomena Institute, Ohio University, Athens, Ohio 45701, USA; nc747821@ohio.edu
[6] Departamento de Física, CEDENNA, Universidad Técnica Federico Santa María, Av. España 1680, Valparaíso 11520, Chile
* Correspondence: myersn1@vt.edu (N.M.M.); francisco.penar@usm.cl (F.J.P.)

Abstract: Graphene is perhaps the most prominent "Dirac material," a class of systems whose electronic structure gives rise to charge carriers that behave as relativistic fermions. In multilayer graphene several crystal sheets are stacked such that the honeycomb lattice of each layer is displaced along one of the lattice edges. When subject to an external magnetic field, the scaling of the multilayer energy spectrum with the magnetic field, and thus the system's thermodynamic behavior, depends strongly on the number of layers. With this in mind, we examine the performance of a finite-time endoreversible Otto cycle with multilayer graphene as its working medium. We show that there exists a simple relationship between the engine efficiency and the number of layers, and that the efficiency at maximum power can exceed that of a classical endoreversible Otto cycle.

Keywords: magnetic cycle; quantum Otto cycle; quantum thermodynamics; graphene

1. Introduction

There is rapidly growing interest in the development of quantum technologies, devices that take advantage of the unique properties of quantum systems to enhance their performance. This, in turn, has led to increased focus on the field of quantum thermodynamics [1–4]. Within the broad spectrum of topics that fall under the umbrella of quantum thermodynamics, significant attention is paid to the study of quantum heat engines - devices that extend the principles of classical heat engines to include working mediums made up of quantum systems [5–9].

Efficiency, defined as the ratio of the net work to the heat absorbed from the hot reservoir, is by far the most prominent metric of engine performance. To maximize engine efficiency the strokes of the cycle must be carried out quasistatically. However, truly quasistatic strokes require infinite time to implement, thus leading to vanishing power output. Practically useful metrics of heat engine performance must therefore account for cycles implemented in finite time. *Endoreversible thermodynamics* [10–12] provides a framework for introducing finite-time behavior by assuming that, while the working medium remains in a state of local equilibrium at all times during the cycle, the heating and cooling strokes occur quickly enough that the working medium never fully thermalizes with the hot and cold reservoirs. A prominent performance characteristic within endoreversible thermodynamics is the *efficiency at maximum power* (EMP) which corresponds to maximizing the power output with respect to the external control parameter and then determining the efficiency at that maximum power output. Endoreversible cycles have also been studied in the context of quantum heat engines. We draw particular attention to Ref. [13], where it was shown that the EMP of an endoreversible Otto cycle with a quantum harmonic oscillator as the working medium exceeds the Curzon-Albhorn (CA) efficiency, the EMP achieved by the Otto cycle with a classical working medium.

 doi:10.20944/preprints202304.0113.v1

When considering possible systems to serve as the working medium of a quantum heat engine, graphene stands out as intriguing candidate. Graphene's optical, electronic, and mechanical properties have been extensively studied in recent years [14–20]. Furthermore, graphene is a prominent Dirac material, systems whose low energy excitations behave as relativistic massless fermions [21]. Thus the study of quantum heat engines with graphene as a working medium can give insight into the role of relativistic quantum features in engine performance [22,23]. In particular, the performance of a quasistatic Otto engine with twisted bilayer graphene was recently studied [24]. In this work it was found that the highest efficiency is reached when the twist angle corresponds to the magic angle of 0.96 degrees. These results show that for a heat engine with multilayer graphene as the working medium the number and configuration of the crystal sheets plays a significant role in the engine performance. Significant attention has also been given to graphene-based engines in the context of continuous, thermoelectric machines [25–28]. Notably, graphene has also been used in the construction of an experimental nanoscale cyclic heat engine [29].

As in Ref.[24] the calculation is quasi-static, assuming that the bilayer always reaches thermodynamic equilibrium at reservoir temperatures and only for the chosen temperatures ($T_{min} =$ 30 K and $T_{max} =$ 100 K) and minimum magnetic field ($B_{min} =$ 5 T). Therefore in this manuscript we analyze the finite time performance of an Otto cycle with multilayer graphene as the working medium using the framework of endoreversible thermodynamics. Additionally, we explore different temperatures and external magnetic fields to determine the efficiency reached at maximum power for each case, and compare these results with the ideal Courzon-Ahlborn efficiency.

In section 2 we provide relevant background, including the analytical results of the energy spectrum for monolayer, bilayer, and trilayer graphene. In section 3 we determine a closed form for the partition function and examine the equilibrium thermodynamic behavior of multilayer graphene. In section 4 we introduce the endoreversible Otto cycle for multilayer graphene before presenting the results for the engine efficiency, power output, and EMP in section 5.

2. Model

In multilayer graphene, the crystal sheets are placed on top of each other in different stacking configurations and are connected through weak van der Waals forces. The stacking configurations are determined by the orientation of the two triangular sublattices that make up the primary honeycomb lattice of a single sheet. For two stacked sheets, three possible orientations, A, B, and C, are possible, each corresponding to displacing one of the sublattice atoms along the edge of the honeycomb with respect to the neighboring sheet [30]. Subject to a perpendicular external magnetic field, these systems can be analyzed using a π-orbital continuum model. Such an analysis is described extensively in Ref. [30]. In our analysis we will focus on two particular stacking configurations. For bilayer graphene we consider Bernal stacking, also known as AB stacking. For the case of trilayer graphene we consider the rhombohedral configuration, also known as ABC stacking [31]. Significantly, an exact analytical result for the energy spectrum as a function of the external magnetic field can be found for these two cases.

2.1. Monolayer Graphene

In monolayer graphene the application of a perpendicular magnetic field results in unevenly spaced Landau levels with an energy spectrum proportional to the root of the level quantum number n [32],

$$E_n = \pm\sqrt{2e\hbar v_f^2 nB},\ n = 0, 1, 2, ..., \tag{1}$$

where B is the magnitude of the magnetic field, e is the electron charge, $\hbar$ is Planck's constant, and v_f is the Fermi velocity ($\sim 10^6$ m/s). Such an energy spectrum is characteristic of ultra-relativistic massless particles with the Fermi velocity playing the role of the speed of light. The positive energy branch corresponds to particle behavior and the negative energy branch to holes [30]. These energy

Preprints (www.preprints.org) | NOT PEER-REVIEWED | Posted: 7 April 2023 doi:10.20944/preprints202304.0113.v1

levels are four times degenerate, including the zero energy state, where the factor of four arises from spin degeneracy and non-equivalent BZ points K and $K^{'}$, known as valley degeneracy.

2.2. Bilayer Graphene: AB stacking

For a bilayer system, the most stable coupling corresponds to Bernal, or AB, stacking. This consists of displacing the A sublattice atoms of the upper layer so that they lie on top of the B sublattice atoms of the lower layer. Notably, the bilayer system has a quadratic dispersion relation, which gives rise to an interesting phenomenon. While the Dirac equation still models the dynamics of the low energy states, the quadratic dispersion relation indicates that the described charge carriers have mass. In this case, under a perpendicular external magnetic field, the low energy spectrum takes the form [33],

$$E_n = \pm\hbar\omega_c\sqrt{n(n-1)},\ n = 0, 1, 2, .. \tag{2}$$

where $\omega_c \equiv eB/m^*$ corresponds to the cyclotron frequency. This effective mass, m^*, is related to the Fermi velocity and the interlayer interaction parameter, $t_\perp$, by $m^* = t_\perp/2v_f^2$. This corresponds to a numerical value of $m^* \sim (0.039 \pm 0.002)\ m_e$, where m_e is the electron rest mass. Note that Eq. (2) has two zero energy levels, corresponding to $n = 0$ and $n = 1$.

2.3. Trilayer Graphene: ABC stacking

Trilayer graphene in the ABC configuration acts as a semiconductor with a gate tunable band gap. The energy spectrum has the form [30],

$$E_n = \pm\frac{\left(2\hbar v_F^2 eB\right)^{3/2}}{t_\perp^2}\sqrt{n(n-1)(n-2)},\ n = 0, 1, 2, ... \tag{3}$$

Note that in the case of trilayer graphene the zero-energy state is 12 fold degenerate, while the other energy states remain fourfold degenerate just as in the bilayer and monolayer case.

Preprints (www.preprints.org) | NOT PEER-REVIEWED | Posted: 7 April 2023 doi:10.20944/preprints202304.0113.v1

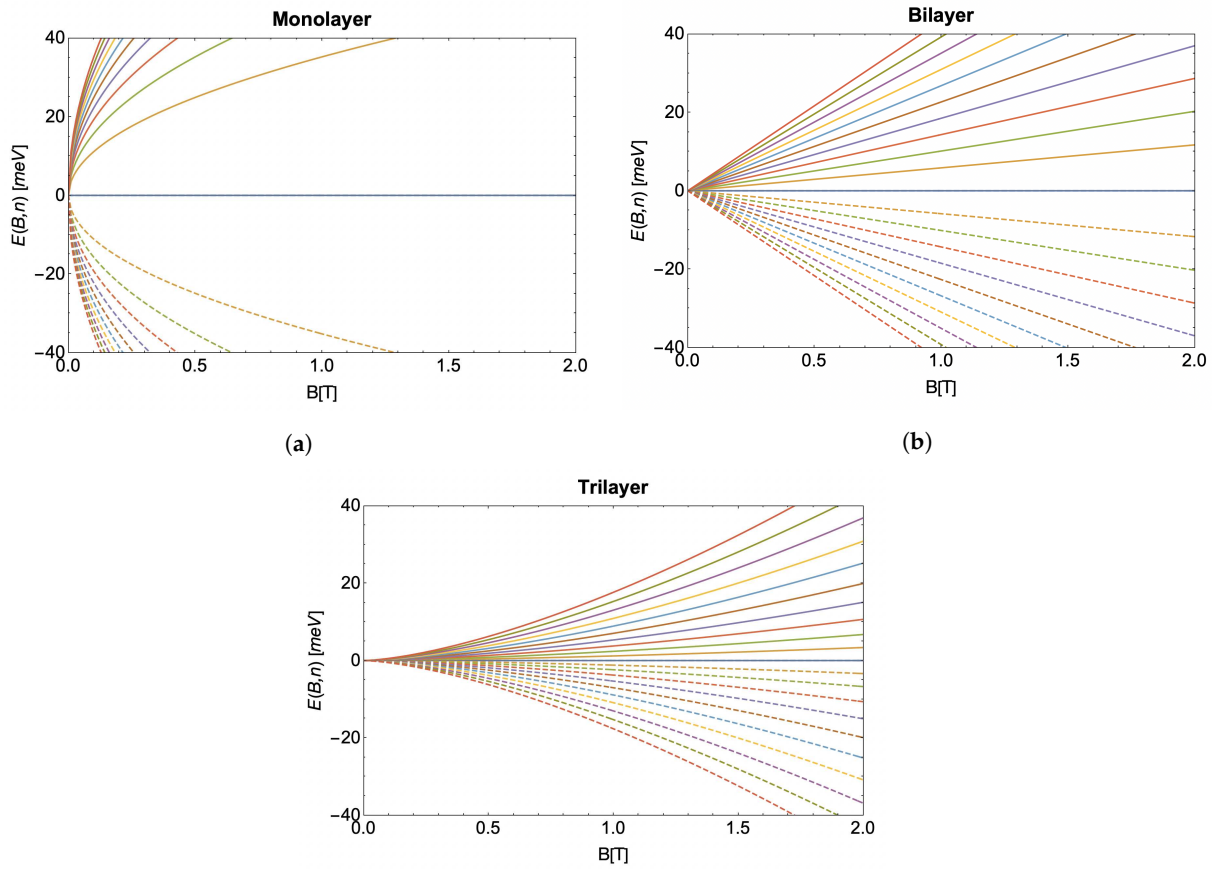

Figure 1. (a–c) Energy spectrum as a function of the external magnetic field for the first 10 Landau levels of (a) monolayer, (b) bilayer (with $m^* = 0.03\ m_e$) and (c) trilayer graphene. Solid (dashed) lines correspond to electrons (holes).

3. Partition Function and Equilibrium Thermodynamics

Comparing the energy spectra presented in the previous section, we see a pattern emerging in how the energy scales with the magnetic field. Each energy is proportional to $B^{\mathcal{N}/2}$ where $\mathcal{N}$ is the number of layers. To illustrate this behavior, we plot the first ten positive and negative energy states as a function of the external field for monolayer, bilayer, and trilayer graphene in Fig. 1. We also see the energy spectra follow a common structure in regard to the quantum number n, which takes the form,

$$f_{\mathcal{N}}(n) = \sqrt{\prod_{k=0}^{\mathcal{N}-1}(n-k)}. \tag{4}$$

Therefore, we can compactly write the energy spectrum for the multilayer system in the form [30],

$$\mathcal{E}_{n,\mathcal{N}} = \theta_{\mathcal{N}} B^{\frac{\mathcal{N}}{2}} f_{\mathcal{N}}(n), \tag{5}$$

where $\theta_{\mathcal{N}} \equiv (2e\hbar v_f^2)^{\mathcal{N}/2}(t_\perp)^{1-\mathcal{N}}$, is a constant that depends on the number of layers and the stacking structure of the system.

Note that the energy spectra in Eqs. (1), (2), and (3) include both positive and negative energy solutions corresponding to electrons and holes, respectively. It is important to highlight that our approximation considers the energy spectra close to the Dirac points of the Brillouin zone, as additional energy solutions require extended approaches not yet fully solved. We focus on the electron excitations

Preprints (www.preprints.org) | NOT PEER-REVIEWED | Posted: 7 April 2023 doi:10.20944/preprints202304.0113.v1

only, similar to established analysis for the case of a twisted bilayer graphene system [24]. This regime can be achieved by gating the monolayer graphene [34] and through moderate electron doping for the case of bilayer [35] and trilayer graphene samples [36]. This makes our restriction to the positive energy solutions experimentally available for the three graphene systems we study.

To accurately determine the partition function, we need to carefully consider the degeneracy of the energy levels, especially for the zero-energy state. The compact form of counting these degenerate states in the partition function is given by,

$$\mathcal{Z} = 4\,(\mathcal{N}-1) + \sum_{n=0}^{\infty} 4\,e^{-\beta\mathcal{E}_{n,\mathcal{N}}}. \tag{6}$$

The partition function for the energy spectrum given in Eq. (5) does not have a simple closed-form solution, except for the case of one layer. However, if we assume that the number of layers $\mathcal{N}$ is not very large compared with the number of states n, then the energy spectrum can be approximated as

$$\mathcal{E}_{n,\mathcal{N}} \approx \theta_{\mathcal{N}} B^{\frac{\mathcal{N}}{2}}\, n^{\frac{\mathcal{N}}{2}}. \tag{7}$$

For large n we can approximate the partition function sum as an integral of the form,

$$\mathcal{Z} \approx 4(\mathcal{N}-1) + 4\int_0^{\infty} dn\, e^{-\beta\theta_{\mathcal{N}} B^{\frac{\mathcal{N}}{2}}\, n^{\frac{\mathcal{N}}{2}}}. \tag{8}$$

Noting that,

$$\int_0^{\infty} dx\, e^{-ax^{\frac{\mathcal{N}}{2}}} = a^{-\frac{2}{\mathcal{N}}}\,\Gamma\left(\frac{2+\mathcal{N}}{\mathcal{N}}\right), \tag{9}$$

we obtain a simple analytical form for the partition function,

$$\mathcal{Z}\,(T,B,\mathcal{N}) = 4(\mathcal{N}-1) + 4\left(\frac{\theta_{\mathcal{N}} B^{\frac{\mathcal{N}}{2}}}{k_B T}\right)^{-\frac{2}{\mathcal{N}}}\Gamma\left(\frac{2+\mathcal{N}}{\mathcal{N}}\right). \tag{10}$$

From the partition function, all relevant equilibrium thermodynamic properties can be determined as follows,

$$\mathcal{F} = -k_B T \ln \mathcal{Z},\ \mathcal{S} = -\left(\frac{\partial \mathcal{F}}{\partial T}\right)_B, \tag{11}$$

$$\mathcal{U} = k_B T^2 \left(\frac{\partial \ln \mathcal{Z}}{\partial T}\right)_B,\ \mathcal{C}_B = \left(\frac{\partial \mathcal{U}}{\partial T}\right)_B, \tag{12}$$

$$\mathcal{M} = -\left(\frac{\partial \mathcal{F}}{\partial B}\right), \tag{13}$$

where $\mathcal{F}$ is the free energy, $\mathcal{S}$ is the entropy, $\mathcal{U}$ is the internal energy, $\mathcal{C}_B$ is the heat capacity, and $\mathcal{M}$ is the magnetization. In Figs. 2 and 3 we compare the internal energy ($\mathcal{U}$) and entropy ($\mathcal{S}$), respectively, for monolayer, bilayer, and trilayer graphene. To ensure that our analytical approximation for the partition function is valid, we also plot the internal energy and entropy determined from numerical calculations of the partition function sum up to 50,000 terms.

Preprints (www.preprints.org) | NOT PEER-REVIEWED | Posted: 7 April 2023 doi:10.20944/preprints202304.0113.v1

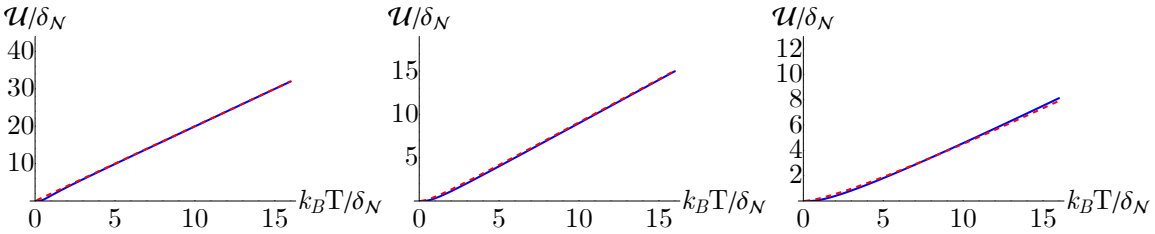

Figure 2. Internal energy as a function of temperature determined from the analytical approximation for the partition function given in Eq. (10) (red, dashed) and from a numerical summation obtained by truncating Eq. (6) after the first 50,000 terms (blue, solid) for (a) monolayer, (b) bilayer and (c) trilayer graphene. Here $\delta_{\mathcal{N}} \equiv \theta_{\mathcal{N}} B^{\mathcal{N}/2}$ such that the plot axes are unitless.

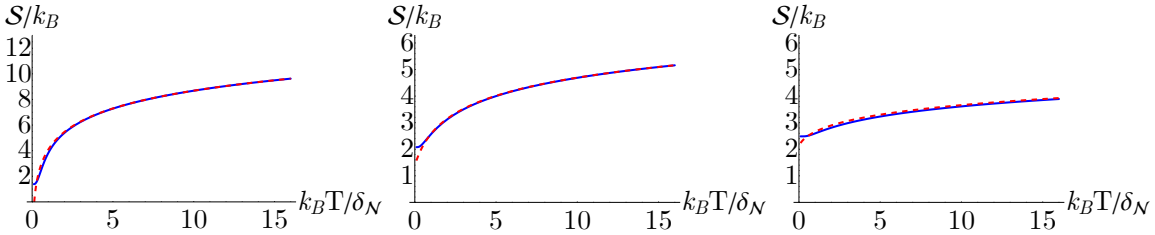

Figure 3. Entropy as a function of temperature determined from the analytical approximation for the partition function given in Eq. (10) (red, dashed) and from a numerical summation obtained by truncating Eq. (6) after the first 50,000 terms (blue, solid) for (a) monolayer, (b) bilayer and (c) trilayer graphene. Here $\delta_{\mathcal{N}} \equiv \theta_{\mathcal{N}} B^{\mathcal{N}/2}$ such that the plot axes are unitless.

4. The endoreversible Otto cycle

The Otto cycle consists of four strokes, illustrated graphically in Fig. 4 using an entropy (S) - magnetic field (B) diagram. The first stroke (A $\rightarrow$ B) is an isentropic compression in which the external field is varied from B_1 to B_2 while the working medium is isolated from the thermal reservoirs. During this stroke an amount of work, W_{comp}, must be supplied to compress the working medium. The second stroke (B $\rightarrow$ C) is an isochoric heating stroke in which the working medium draws an amount of heat, Q_{in}, from the hot reservoir while the external field is held constant. The third stroke (C $\rightarrow$ D) is an isentropic expansion where the working medium is again disconnected from the thermal reservoirs and the external field is varied from B_2 back to B_1. During this stroke an amount of work, W_{exp}, is extracted from the expansion of the working medium. The final stroke (D $\rightarrow$ A) is an isochoric cooling stroke in which the working medium expels and amount of heat, Q_{out} to the cold reservoir while the external field is held constant. Note that the work parameter (B) plays the role of an *inverse* volume, increasing during the compression stroke (A $\rightarrow$ B) and decreasing during the expansion stroke (C $\rightarrow$ D).

Characteristic of the framework of endoreversibility, we will assume the working medium remains in a state of local equilibrium throughout the cycle, but, due to finite-time thermalization strokes, never achieves global equilibrium with the reservoirs. The thermodynamic equation of state for the internal energy of working medium at each corner of the cycle must thus be expressed in terms of the corresponding temperature, T_A, T_B, T_C, or T_D, and the external field strength, B_1 or B_2. Ultimately, we want to determine expressions for the engine performance figures of merit solely in terms of the experimentally controllable parameters, namely the temperatures of the thermal reservoirs, T_l and T_h, the magnetic field strengths B_1 and B_2, and the durations of the heating and cooling strokes, τ_h and τ_l. In order to do so, we must model the thermal conduction during the isochoric strokes and apply the constraint that the entropy remains constant during the isentropic strokes. For this endoreversible analysis we will follow the procedure established in Ref. [13].

Preprints (www.preprints.org) | NOT PEER-REVIEWED | Posted: 7 April 2023 doi:10.20944/preprints202304.0113.v1

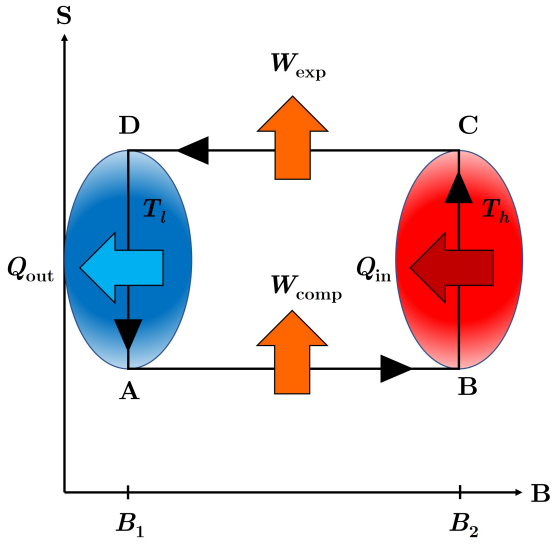

Figure 4. Entropy (S) versus external field (B) diagram for the Otto Cycle. Note that the system is only in contact with the thermal reservoirs during the isochoric (vertical) strokes. Note that in the endoreversible framework the working medium does not fully thermalize to the temperatures T_h and T_l of the hot and cold reservoirs at points C and A, respectively. Here Q_{in} is the amount of heat drawn from the hot reservoir during the heating stroke (B $\rightarrow$ C) and Q_{out} is the amount of heat expelled to the cold reservoir during the cooling stroke (D $\rightarrow$ A). Similarly, W_{comp} is the amount of work supplied to the working medium during the compression stroke (A $\rightarrow$ B), while W_{exp} is the amount of work extracted from the working medium during the expansion stroke (C $\rightarrow$ D).

During the isentropic compression stroke (A $\rightarrow$ B) the working medium is decoupled from the thermal reservoirs. As such, all change in the working medium's internal energy can be associated with work,

$$W_{\text{comp}} = U_{\text{B}}(T_{\text{B}}, B_2) - U_{\text{A}}(T_{\text{A}}, B_1). \tag{14}$$

During the isochoric heating stroke (B $\rightarrow$ C), the external field is held constant. Thus the difference in internal energy can be associated entirely with heat,

$$Q_{\text{in}} = U_{\text{C}}(T_{\text{C}}, B_2) - U_{\text{B}}(T_{\text{B}}, B_2). \tag{15}$$

As mentioned above, unlike in the quasistatic case, $T_{\text{C}} \neq T_h$ since the working medium does not fully thermalize with the hot reservoir. As the heating stroke is now carried out in finite time, we must determine how the temperature of the working medium changes during the duration of the stroke. The temperatures T_{B} and T_{C}, corresponding to the temperature of the working medium at the beginning and ending of the heating stroke, respectively, must satisfy the conditions,

$$T(0) = T_{\text{B}}, \quad T(\tau_h) = T_{\text{C}} \quad \text{and} \quad T_{\text{B}} < T_{\text{C}} \leq T_h, \tag{16}$$

where τ_h is the duration of the heating stroke. Consistent with the assumptions of endoreversibility, we model thermal conduction in the working medium using Fourier's law. In this case, the temperature change from T_{B} to T_{C} can be found by applying Newton's law of cooling,

$$\frac{dT}{dt} = -\alpha_h \left(T(t) - T_h\right), \tag{17}$$

Preprints (www.preprints.org) | NOT PEER-REVIEWED | Posted: 7 April 2023 doi:10.20944/preprints202304.0113.v1

where α_h is a constant that depends on the thermal conductivity and heat capacity of the working medium. Solving Eq. (17) yields,

$$T_{\mathrm{C}} - T_h = (T_{\mathrm{B}} - T_h)e^{-\alpha_h \tau_h}. \tag{18}$$

Just as in the compression stroke, the work extracted during the isentropic expansion stroke (C $\rightarrow$ D) is found from,

$$W_{\mathrm{exp}} = U_{\mathrm{D}}(T_{\mathrm{D}}, B_1) - U_{\mathrm{C}}(T_{\mathrm{C}}, B_2). \tag{19}$$

During the isochoric cooling stroke (D $\rightarrow$ A) the heat exchanged with the cold reservoir is given by,

$$Q_{\mathrm{out}} = U_{\mathrm{A}}(T_{\mathrm{A}}, B_1) - U_{\mathrm{D}}(T_{\mathrm{D}}, B_1), \tag{20}$$

where, in analogy to the heating stroke, T_{A} and T_{D} satisfy the conditions,

$$T(0) = T_{\mathrm{D}} \quad \text{and} \quad T(\tau_l) = T_{\mathrm{A}} \quad \text{with} \quad T_{\mathrm{D}} > T_{\mathrm{A}} \geq T_l. \tag{21}$$

We again apply Fourier's law and Newton's law of cooling to model the temperature change during the stroke,

$$\frac{dT}{dt} = -\alpha_l \left(T(t) - T_l\right), \tag{22}$$

which after solving yields,

$$T_{\mathrm{A}} - T_l = \left(T_{\mathrm{D}} - T_l\right) e^{-\alpha_l \tau_l}. \tag{23}$$

With expressions for the work done and heat exchanged during each stroke of the cycle we can now determine the cycle efficiency,

$$\eta = -\frac{W_{\mathrm{comp}} + W_{\mathrm{exp}}}{Q_{\mathrm{in}}}, \tag{24}$$

and power output,

$$P = -\frac{W_{\mathrm{comp}} + W_{\mathrm{exp}}}{\gamma(\tau_h + \tau_l)}. \tag{25}$$

Note that γ is a multiplicative factor that implicitly incorporates the duration of the isentropic strokes [13].

By definition, the entropy remains constant during the isentropic strokes. We can use this fact to obtain a relationship between the initial and final temperatures and magnetic field strengths during the isentropic strokes. Using $dS(T, B) = 0$ we obtain the following first order differential equation,

$$\frac{dB}{dT} = -\frac{\left(\frac{\partial S}{\partial T}\right)_B}{\left(\frac{\partial S}{\partial B}\right)_T}. \tag{26}$$

Taking the partial derivatives of the entropy found from Eq. (11) we arrive at,

$$\frac{dB}{dT} = \frac{2B}{\mathcal{N}T}. \tag{27}$$

Solving Eq. (27) for the compression stroke we find,

$$\frac{T_{\mathrm{A}}}{T_{\mathrm{B}}} = \left(\frac{B_1}{B_2}\right)^{\frac{\mathcal{N}}{2}}. \tag{28}$$

 doi:10.20944/preprints202304.0113.v1

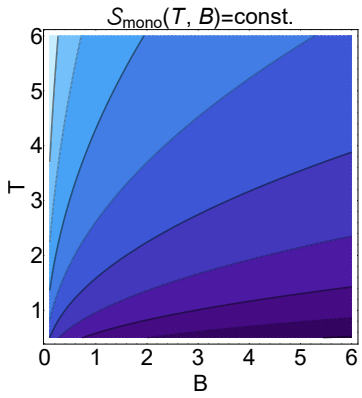

(